PAPER

Refractive index sensor based on high-order surface plasmon resonance in gold nanofilm coated photonic crystal fiber

Refractive index sensor based on high-order surface plasmon resonance in gold nanofilm coated photonic crystal fiber*

Zhen-Kai Fan(范振凯)[1], Shao-Bo Fang(方少波)[3,4,†], Shu-Guang Li(李曙光)[2], and Zhi-Yi Wei(魏志义)[3,4]

[1] School of Information Science and Engineering, Hebei University of Science and Technology, Shijiazhuang 050018, China
[2] State Key Laboratory of Metastable Materials Science and Technology, and Key Laboratory of Microstructural Material Physics of Hebei Province, School of Science, Yanshan University, Qinhuangdao 066004, China
[3] Institute of Physics, Chinese Academy of Sciences, Beijing 100190, China
[4] University of Chinese Academy of Sciences, Beijing 100049, China

(Received 22 January 2019; revised manuscript received 9 June 2019; published online 7 August 2019)

We propose a novel kind of wide-range refractive index optical sensor based on photonic crystal fiber (PCF) covered with nano-ring gold film. The refractive index sensing performance of the PCF sensor is analyzed and simulated by the finite element method (FEM). The refractive index liquid is infiltrated into the cladding air hole of the PCF. By comparing the sensing performance of two kinds of photonic crystal fiber structures, a wide range and high sensitivity structure is optimized. The surface plasmon resonance (SPR) excitation material is chose as gold, and large gold nanorings are embedded around the first cladding air hole of the PCF. The higher order surface plasmon modes are generated in this designed optical fiber structure. The resonance coupling between the fundamental mode and the 5th order surface plasmon polariton (SPP) modes is excited when the phase matching condition is matched. Therefore, the 3rd loss peaks appear obvious red-shift with the increase of the analyte refractive index , which shows a remarkable polynomial fitting law. The fitnesses of two structures are 0.99 and 0.98, respectively. When the range of refractive indices is from 1.40 to 1.43, the two kinds of sensors have high linear sensitivities of 1604 nm/RIU and 3978 nm/RIU, respectively.

Keywords: surface plasmon resonance, photonic crystal fiber, sensor

PACS: 42.81.Pa, 42.81.Gs, 07.07.Df **DOI:** 10.1088/1674-1056/ab327a

1. Introduction

Surface plasmon resonance (SPR)[1–3] refractive index sensor based on photonic crystal fiber (PCF) has attracted extensive attention from a large number of researchers, which is due to the more important science application compared to the traditional fiber.[4] A significant loss peak is excited at the resonance wavelength and an extremely high sensitivity of the liquid analytes is obtained. The phase matching is satisfied between the fundamental mode and the surface plasmon polariton (SPP) modes, and the surface plasmon resonance (SPR) can be obtained. Thus, when the phase match between the fundamental mode and the SPP mode is met in the designed PCF, the SPR will occur. It has been widely used in the field of SPR-PCF refractive index sensor.[5] While the metals of aluminum, copper, and silver have weak chemical stability, the more stable metal gold is selected as the SPR material. There are usually two ways to induce the SPR in the PCF. They are metal film coating and metal nano-wire filling in the air holes of the designed PCF.[6,7] The SPR based sensing technology has been widely applied in the study of bimolecular interactions, tracking and identifying target analytes, medical pharmacy, environmental testing, and biochemical technology.[8–10]

In the past decade, various types of SPR-PCF refractive index sensors have been researched and investigated to promote the detecting technology of optical fiber. The covering technology of gold nanofilm is applied on the fabrication of the SPR fiber refractive index sensors, and some significant progresses have been made. Chen *et al.*[11] proposed a kind of surface plasmon resonance sensor based on a novel D-shaped photonic crystal fiber for low refractive index detection. The maximum spectral sensitivity of the SPR-PCF is as high as 11055 nm/RIU, but its detection range is very narrow. Lu *et al.*[12] presented a D-shaped PCF plasmonic refractive index sensor based on the gold grating. The gold grating was introduced to modulate the resonance wavelength and enhance the refractive index sensitivity. Yang *et al.*[13] proposed a novel kind of SPR sensor based on concave-shaped PCF for the low refractive index detection. The maximum wavelength sensitivity of the refractive index sensor is 1700–10700 nm/RIU when the refractive index ranges from 1.19 to 1.29. Liu *et al.*[14] reported a high birefringent PCF based SPR sensor for a broad range of low refractive index detection. The maximum wavelength sensitivity is 6300 nm/RIU for the broad refractive index detection range from 1.00 to 1.43. Luan *et al.*[15] an-

*Project supported by the National Key Research and Development Program of China (Grant No. 2017YFC0110301), the National Natural Science Foundation of China (Grant Nos. 61575219, 91850209, and 11434016), the College Young Talents Program of Hebei Province, China (Grant No. BJ2018040), the Hebei University of Science and Technology Talent Introduction Project, China (Grant No. 1181324), and the Youth Innovation Promotion Association, Chinese Academy of Sciences (Grant No. 2018007).

†Corresponding author. E-mail: shaobo.fang@iphy.ac.cn

alyzed a kind of high refractive index plasmonic sensor based on D-shaped PCF with laterally accessible hollow core. Compared with the traditional PCF-based SPR sensors, the proposed sensor can be conveniently coated with metal films and provide a possibility for real time detecting. Chu *et al.*[16] designed a SPR based photonic quasi-crystal fiber biosensor for high refractive index liquid analytes. The sensor exhibited the linear detecting performance with a maximum refractive index sensitivity of 4400 nm/RIU. These reported research efforts all aim at obtaining a higher detection sensitivity of refractive index. While our designed structure is novel by covering the large gold nanofilm in the first cladding air holes of the SPR based PCF and our designed structure is primarily to obtain a wide-range and high sensitivity sensing performance for the refractive index liquid analyte by utilizing the gold film coating technology.

In this paper, two wide-range and high sensitivity photonic crystal based SPR refractive index sensors are proposed and researched by the finite element method (FEM). The first cladding air hole of PCF is coated by a large gold nanofilm. As this method of covering gold results in a great increase in the surface area of the metal, more surface electrons are in contact with the photon energy of the PCF core. The SPR is significantly enhanced between the fundamental mode and the 5th order SPP modes. The loss spectral characteristics of the SPR-PCF are numerically studied by the commercial mode solver. It is observed that three loss peaks occur in the wavelength range. In the design, a novel kind of high order SPP modes is obtained by the simulation. As the phase matching condition between the 5th order SPP modes and the fundamental mode is met, the SPR for the 5th order SPP modes and the fundamental mode is obtained. The 3rd loss peak of the type-1 and 2 exhibits better sensitivity to the analyte refractive index. The wide-range sensitivity of the PCF coincidences a polynomial fit, and there is a high sensitivity when the detecting range is from 1.33 to 1.43. When the sensing ranges are from 1.33 to 1.39 and from 1.40 to 1.43 for type-2, the resonance wavelength dependance on the refractive index of analyte liquid follows a linear fitting law. The relatively high sensitivity of 3978 nm/RIU is obtained.

2. Theory and method

The cross-section of the proposed SPR based PCF refractive index sensor with the wide range is shown in Figs. 1(a) and 1(b). The cladding of the photonic crystal fiber structure consists of two layers of air holes, and the core of the fiber is formed to obtain air holes by removing the center of the structure. All air holes are arranged in a hexagonal lattice with a lattice constant of 2.0 μm. This outermost air hole is selected as the liquid analyte channel, which is infiltrated by the liquid to be measured. The radii of the air hole and liquid analyte are d_2 and d_1, respectively. The d_1 is 1.0 μm and 1.6 μm for the two structures in Figs. 1(a) and 1(b). This large metal film is covered around the first cladding air hole, and its thickness is 40 nm. The background material is pure silicon. A perfect matching layer of several microns is added to the outermost layer to absorb excess energy. The loss and refractive index of the fundamental mode dependance on the operation wavelength are shown in Figs. 1(c) and 1(d). The optical performances of the two PCFs can be demonstrated by investigating the variation of limiting loss and effective refractive index. We can find from Fig. 1(c) that three kinds of loss peaks appear, which are due to the resonance couplings between the three kinds of SPP modes and the fundamental mode. From Fig. 1(d), we find only the 2nd and 3rd peaks, while the 1st peak does not appear in the displayed band. This is due to the phase matching between different higher order SPPs and the fundamental mode. In this paper, we study the sensitivity of the 3rd peak to the refractive index of the analyte. It can be seen that the refractive index curve shows a reverse jump. The resonance coupling for the SPP mode and the fundamental mode will be obtained when the phase matching for the 5th order SPP mode and the fundamental mode is satisfied. Therefore, the refractive index sensor based on SPR-PCF can be designed by increasing the analyte refractive index in type-1 and type-2. As shown in Figs. 1(a) and 1(c), the analyte refractive index liquid is infiltrated into the outermost layer of the cladding air hole. We can observe that the three peaks have more obvious blue shifts for type-2 compared with type-1. The effective refractive index of three higher order surface plasmon modes is increased for type-2 by increasing the diameter of the outermost air hole. In the simulation process, this scattering boundary condition and the finite element mesh are set in the fiber mode solver. The background material of the designed two PCFs is pure silica, whose dispersion can be expressed by the Sellmeier dispersion equation

$$n(\lambda) = \sqrt{1 + \frac{{B_1}^2}{\lambda^2 - C_1} + \frac{{B_2}^2}{\lambda^2 - C_2} + \frac{{B_3}^2}{\lambda^2 - C_3}}, \tag{1}$$

where λ is the free space wavelength. The wavelength is in units of μm. We can refer to the fitting constants of B_1, B_2, B_3, C_1, C_2, and C_3 in Ref. [17]. A gold nano-film of dozens of nanometers is covered around the first cladding air hole of the designed two PCFs in this simulation process. However, we can fabricate photonic crystal fibers by magnetron sputtering coating technology in the experimental process. Then, we can fabricate the designed two PCFs by drawing the prefabricated rods in the drawing tower. The simulation can be used to solve the mode of the two PCFs. The optical transmission characteristics of the PCF are researched and investigated by using the mode solver software based on FEM. Furthermore, the confinement loss is one of the key parameters to test the

transmission performance of the PCF, which can be expressed by the formula[18]

$$L_{\mathrm{C}} = 8.686 \times \frac{2\pi}{\lambda} \mathrm{Im}[n_{\mathrm{eff}}] \times 10^4, \tag{2}$$

where λ is the wavelength of the incident light in vacuum in units of μm, $\mathrm{Im}[n_{\mathrm{eff}}]$ represents the imaginary part of the effective refractive index, which is proportional to L_{C}. Therefore, we can obtain the numerical variation law of limiting loss by calculating the effective refractive index of the designed PCF. There are a large number of free-moving electrons on the surface of metals, which have an inherent oscillation frequency. When the photon frequency matches the vibration frequency of the free electrons, the surface plasma is obtained and attenuates on the metal surface. A gold nanofilm is chosen as the SPR excited materials in this model, and the dielectric function of gold is defined by the Drude model[19]

$$\varepsilon_{\mathrm{gold}} = \varepsilon_\infty - \frac{\omega_{\mathrm{D}}^2}{\omega(\omega + \mathrm{j}\gamma_{\mathrm{D}})} - \frac{\Delta\varepsilon \cdot \Omega_{\mathrm{L}}^2}{(\omega^2 - \Omega_{\mathrm{L}}^2) - \mathrm{j}\Gamma_{\mathrm{L}}\omega}, \tag{3}$$

where $\varepsilon_{\mathrm{gold}}$ represents the dielectric constant of gold, ε_∞ represents the permittivity at high frequencies, ω is the angular frequency, ω_{D} is the plasmon frequency, γ_{D} is the damping frequency, and $\Delta\varepsilon$ is the weighting factor. The parameters ε_∞, ω_{D}, γ_{D}, Ω_{L}, and Γ_{L} have been given in Ref. [20]. The thickness of the gold nano-film is set to a constant of 40 nm, and the dielectric properties of gold are set in the fiber mode solution software.

The electric field distributions of the fundamental modes, the 5th order SPP modes, and the resonance coupling mode of the 5th order SPP mode and the fundamental mode are shown in Fig. 2. Figures 2(a)–2(c) present the three optical fiber modes in the type-1 PCF. Figures 2(d)–2(f) show the three fiber modes in the type-2 PCF. When the phase matching between the fundamental mode and the 5th order SPP modes is satisfied, the resonance coupling between the fundamental mode and the 5th order SPP modes is obtained. Then, the energy of the fundamental mode is transferred to the large gold nano-film surface, which forms the resonance coupled modes. Three resonance peaks appear in the loss spectra due to the resonance coupling of three different higher order surface plasmon modes with the fundamental mode of the PCF. In our work, the resonance coupling can be generated between the 5th order SPP modes and the fundamental mode rather than the common 2nd SPP modes.[21,22] The 3rd resonance loss peak has the high sensitivity to the refractive index of the filled analyte liquid. As the analyte refractive index increases, the loss peak will regularly red-shift and the analyte refractive index can be detected by analyzing the loss spectrum. Therefore, the PCF can be used as a waveguide in the field of refractive index sensor.

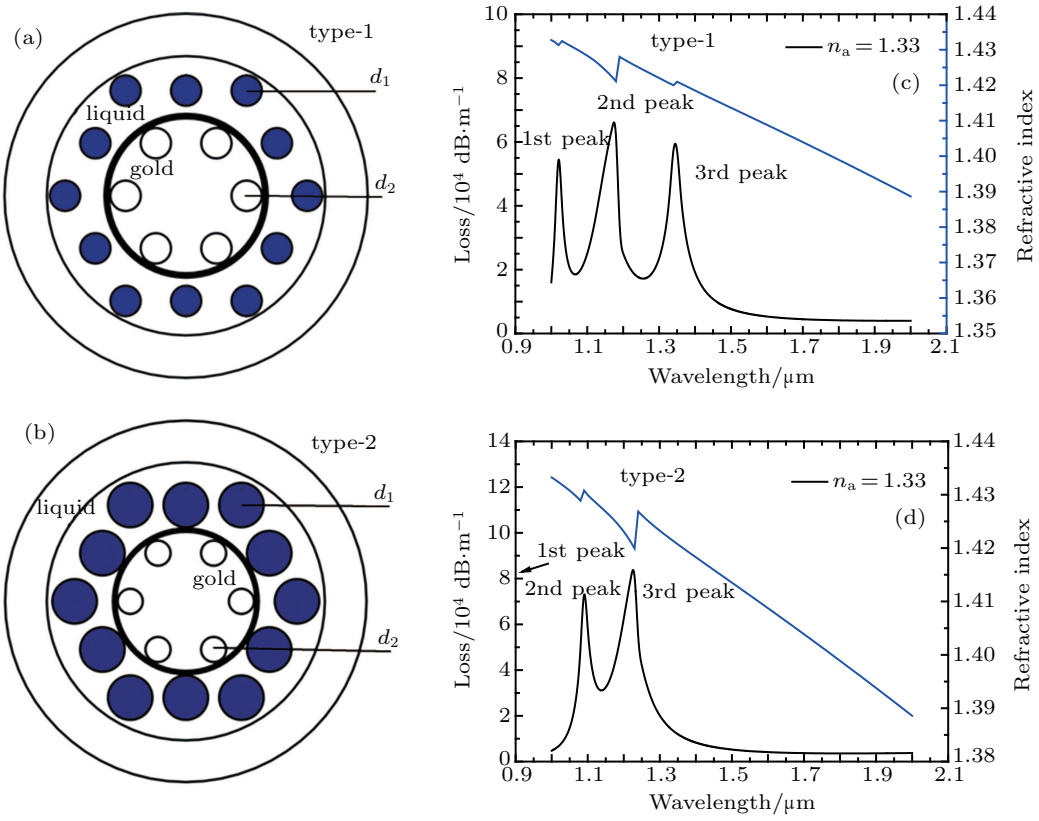

Fig. 1. The cross-sections of the proposed SPR-PCF refractive index sensors of (a) type-1 and (b) type-2. The loss and refractive index of the PCF dependance on the operation wavelength when the analyte refractive index n_a is 1.33 for (c) type-1 and (d) type-2. The outermost layer of the air hole is filled with refractive index analyte.

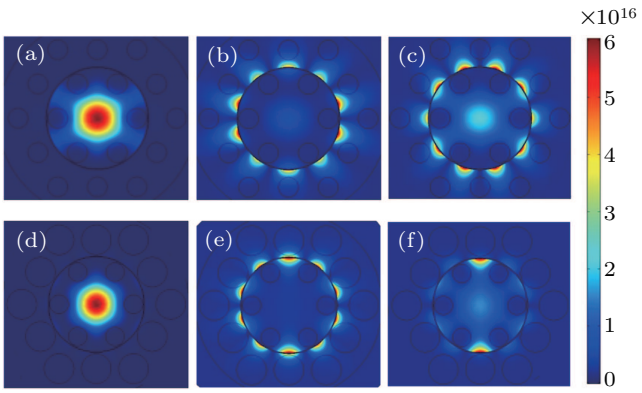

Fig. 2. The electric field distributions of (a) the fundamental mode, (b) the 5th order SPP mode, and (c) the resonance coupled mode of the 5th order SPP mode and the fundamental mode for structure 1. Those of (d) the fundamental mode, (e) the 5th order SPP mode, (f) the SPR modes of the 6th order and the fundamental mode for structure 2.

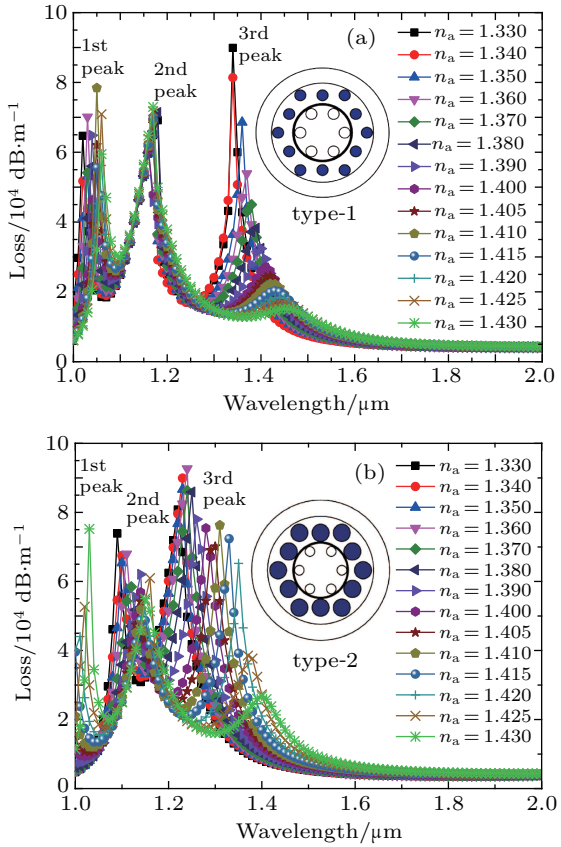

Fig. 3. The losses of the two kinds of SPR-PCF refractive index sensors dependance on the operation wavelength when the analyte refractive index is from 1.33 to 1.43 for (a) type 1 and (b) type 2.

Figure 3 shows the loss of SPR-PCF refractive index sensor dependance on the operation wavelength as the analyze refractive index increases for type-1 and 2. It is observed from Figs. 3(a) and 3(b) that three loss peaks appear in the whole loss spectrum. The 3rd loss peaks show a regular high sensitivity red-shift as the refractive index increases. Therefore, the designed two PCFs will exhibit an excellent sensing performance for the analyte liquid through analyzing numerically the simulated loss spectroscopy. As shown in Figs. 3(a)and 3(b), it is found that the movement of the 3rd peaks is most remarkable. This is attributed to the fact that the resonance coupling between the 5th order SPP mode and the fundamental mode is the strongest compared to the SPR between the other order SPP mode and the fundamental mode. Two optical fiber structures are mosaic to Figs. 3(a) and 3(b), respectively. Here, the 1s, the 2nd, and the 3rd peaks correspond to the resonance coupling of three kinds of SPP modes and the fundamental mode, respectively. The first loss peak is generated by the seventh-order SPR, and the 2nd loss peak is obtained from the sixth-order SPR. As the outermost air holes of the type-2 PCF are enlarged, more liquid is infiltrated into these air holes. These liquids have a strong ability to absorb light energy, resulting in a stronger sensitivity of the third loss peak to the refractive index of the analytes.

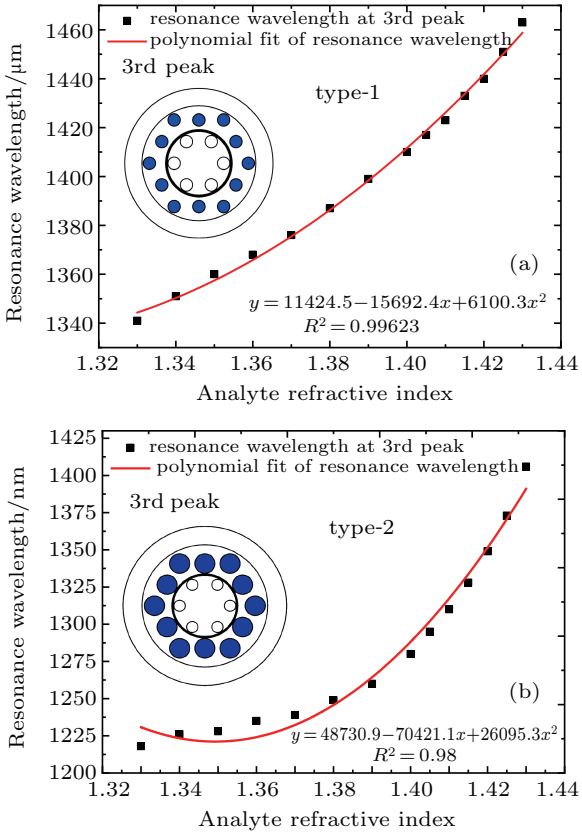

Fig. 4. The resonance wavelength dependance on the analyte refractive index for the 3rd peaks in (a) type-1 and (b) type-2. The fitting formulas of the 3rd peaks are given.

Figure 4 shows the resonance wavelength in the 3rd peak dependance on the analyte refractive index for the designed SPR-PCFs of type-1 and 2. It is very obvious that there is no good linear relationship between the resonance wavelength and the analyte refractive index when the refractive index range is from 1.33 to 1.43. As shown in Figs. 4(a) and 4(b), the resonance wavelength in the 3rd peak gradually red-shifts as the analyte refractive index increases. We can see from Fig. 4 that the high goodness of fit in the 3rd peak is 0.99 and 0.98 by performing a polynomial fit between the resonance wavelength and the analyte refractive

index. The sensitivity formulas of the 3rd peaks for type-1 and 2 are expressed as $y_1 = 3829.8 - 4460.5x + 1766.0x^2$ and $y_2 = 48730.9 - 70421.1x + 26095.3x^2$, respectively. As shown in Figs. 4(a) and 4(b), we can detect the corresponding analyte refractive index by analyzing the resonance wavelength when the refractive index range is from 1.33 to 1.43. It can be found from Figs. 4(a) and 4(b) that the sensitivity of the 3rd peak is much higher compared to that of the 1st and 2nd peaks. According to the resonance wavelength versus the analyte refractive index in the 3rd peak, two PCF refractive index sensors with different sensitivity are obtained. It can be flexibly tuned according to the different detection sensitive requirement. Moreover, the refractive index sensors with two different structures have relatively wide measuring ranges of refractive index.

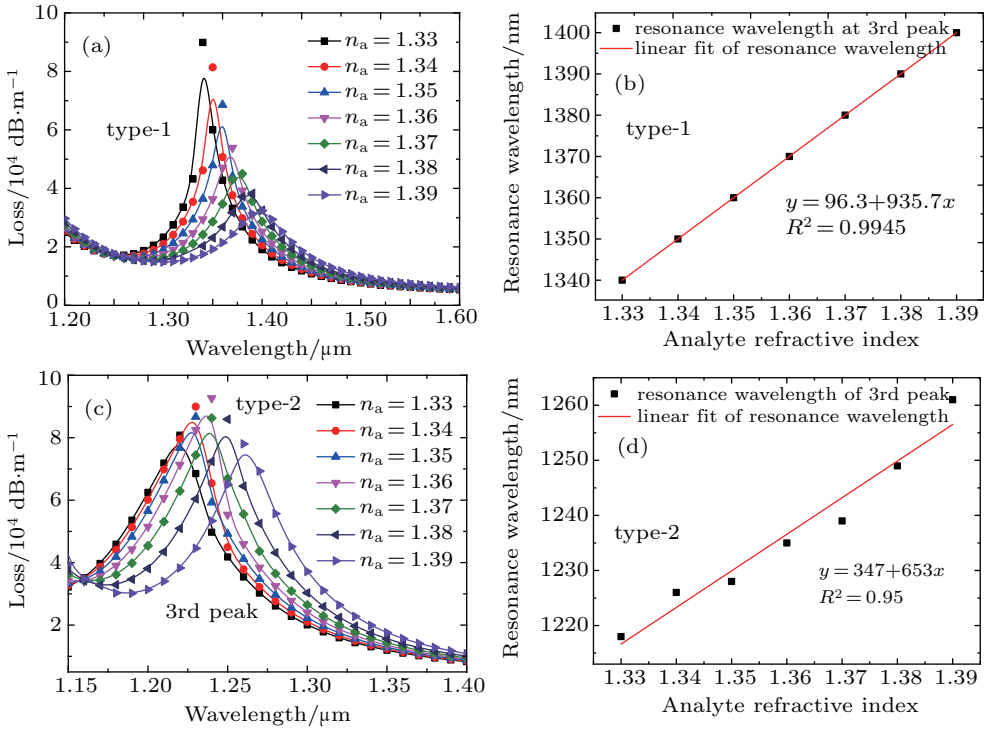

Fig. 5. The loss of the fundamental mode dependance on the operation wavelength for (a) type-1 and (c) type-2, when the analyte refractive index n_a is 1.33, 1.34, 1.35, 1.36, 1.37, 1.38, and 1.39. The resonance wavelength dependance on the analyte refractive index for (b) type-1 and (d) type-2.

Table 1. Resonance wavelength for different analyte for type-1 and type-2 for 3rd peak.

Analyte/RIU	1.330	1.340	1.350	1.360	1.380	1.390	1.400
RW of type-1/μm	1.340	1.350	1.360	1.370	1.380	1.390	1.400
RW of type-2/μm	1.218	1.226	1.229	1.237	1.239	1.248	1.261

The dependence of the loss of the fundamental mode on the operation wavelength for the 3rd peaks in type-1 and 2 is shown in Figs. 5(a) and 5(b) when the analyte refractive index increases from 1.33 to 1.39, respectively. The resonance wavelength of the 3rd peaks dependance on the analyte refractive index is shown in Figs. 5(c) and 5(d), respectively. It can be found that the linear relationship is satisfied. The resonance coupling between the 5th order SPP mode and the fundamental mode is generated, as the phase matching between the 5th order SPP mode and the fundamental mode is met. The energy of the PCF core is transferred to the surface of the large gold nano-film, which leads to the appearance of the 3rd peak. We can see from Fig. 5(a) that the 3rd loss peak of type-1 is gradually moving toward the long wavelength direction as the analyte refractive index increases from 1.33 to 1.39. The losses are 77431.1 dB/m, 70333.8 dB/m, 61211.9 dB/m, 50544.3 dB/m, 43904.2 dB/m, 37503.6 dB/m, and 31582.0 dB/m at the resonance wavelengths of 1.342 μm, 1.351 μm, 1.360 μm, 1.368 μm, 1.376 μm, 1.387 μm, and 1.399 μm, respectively. However, the intensity at the resonance wavelength is gradually reduced. The relationship of the resonance wavelength to the analyte refractive index is expressed as $y = 96.3 + 935.7x$, which shows a high linearity $R_2 = 935.7$ nm/RIU. The average sensitivity of the resonance wavelength to the analyte refractive index is 935.7 nm/RIU as shown in Fig. 5(b). As shown in Fig. 5(c), the 3rd peak of type-2 shows a regular red-shift as the analyte refractive index n_a increases from 1.33 to 1.39. It is very obvious that these resonances occur at 1.218 μm, 1.226 μm, 1.228 μm, 1.235 μm, 1.239 μm, 1.249 μm, and 1.261 μm,

respectively and the resonance intensities are 77047.3 dB/m, 84853.9 dB/m, 81704.6 dB/m, 86962.3 dB/m, 81397.6 dB/m, 80343.4 dB/m, and 74485.2 dB/m, respectively. As shown in Fig. 5(d), the linear fit of the resonance wavelength to the analyte refractive index is calculated and the linear equation is expressed as $y = 96.3 + 935.7x$. A high linearity R_2 is 0.99. The average sensitivity of the resonance wavelength of the 3rd peak to the analyte refractive index from 1.33 to 1.39 is 935.7 nm/RIU. Compared with type-1, the sensitivity of the 3rd peak is relatively low in the refractive index range from 1.33 to 1.39. This second cladding air hole is enlarged for the photonic crystal fiber of type-2, which results in more analyte liquids infiltrating into the optical fiber air hole, compared with the case in type-1. In the low refractive index range, the type-2 PCF exhibits a lower sensitivity to liquid analytes. The outermost air hole of type 2 is filled with more liquid, but its surface plasmon resonance is relatively weak compared with that in type-1. Therefore, the type-1 PCF exhibits better detection sensitivity at low refractive index. Resonance wavelengthes for different analyte refractive indexes for type-1 and 2 are shown in Table 1. The difference of resonance sensitivity between the two structures can be more clearly observed.

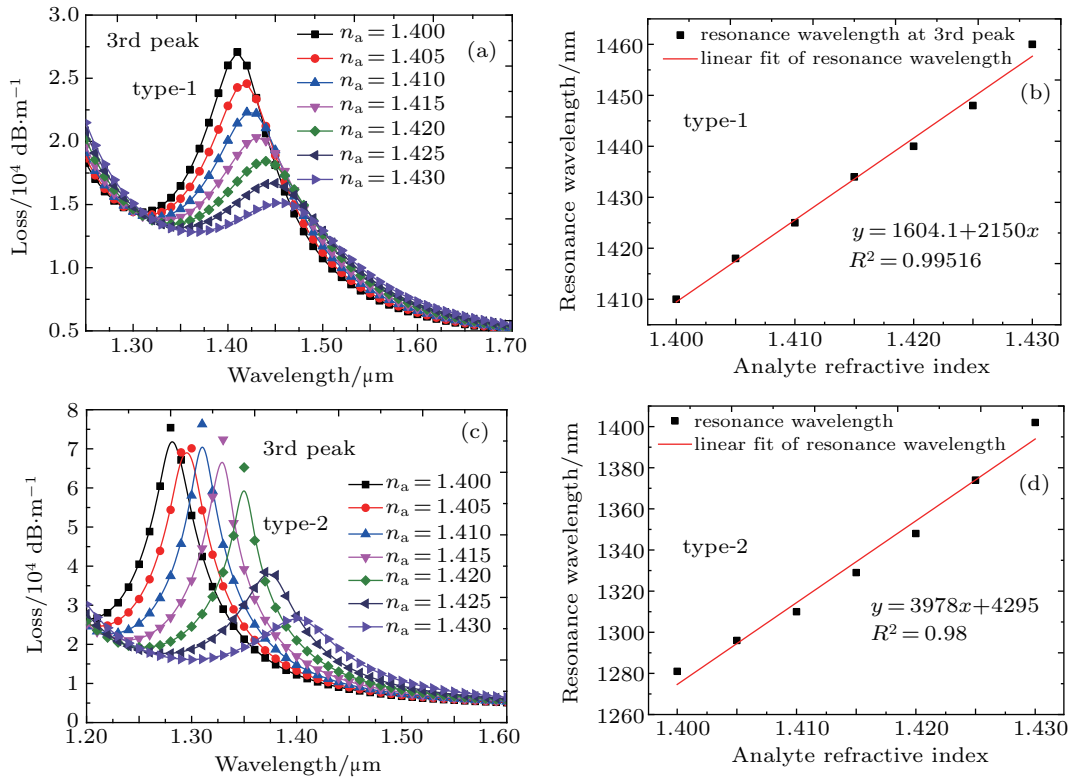

Fig. 6. The loss of the fundamental mode dependance on the operation wavelength for (a) type-1 and (c) type-2 in 3rd peak, when the analyte refractive index increases from 1.400 to 1.430 by a step of 0.005. The resonance wavelength dependance on the analyte refractive index for (b) type-1 and (d) type-2 in 3rd peaks.

Table 2. Resonance wavelength for different analyte for type-1 and type-2 for 3rd peak.

Analyte/RIU	1.400	1.405	1.410	1.415	1.420	1.425	1.430
RW of type-1/μm	1.410	1.418	1.425	1.434	1.440	1.448	1.460
RW of type-2/μm	1.218	1.296	1.310	1.329	1.350	1.375	1.403

Figures 6(a) and 6(b) show the losses of the fundamental mode for the 3rd peak of type-1 dependance on the operation wavelength in the gold nanofilm coated PCF when the analyte refractive index increases from 1.400 to 1.430. The losses of the 3rd peak move towards the long wavelength direction, and their peak values are 26734.4 dB/m, 24404.9 dB/m, 22191.6 dB/m, 20137.9 dB/m, 18359.9 dB/m, and 16625.5 dB/m at the resonance wavelengths of 1.410 μm, 1.418 μm, 1.425 μm, 1.434 μm, 1.440 μm,1.448 μm, and 1.460 μm, which shows a gradual decrease in the resonance intensity. The resonance wavelength versus the analyte refractive index is defined as $y = 1604 + 2150x$, and the high linearity R_2 is 0.99. Figures 6(c) and 6(d) show the resonance wavelength of the 3rd peak of type-2 dependance on the analyte refractive index. The dependance of this resonance wavelength on the analyte refractive index is expressed as $y = 4295 + 3978x$, which is a typical linear relationship by using the method of linear fit. A high linearity of R_2 is obtained as 0.98, and the average sensitivity is 3978 nm/RIU. We can see from Fig. 6(c) that the loss of the 3rd peak of type-2

shows the regular red-shift, and the resonance intensity is reduced regularly. The loss 3rd peak values are 71920.2 dB/m, 69391.8 dB/m, 70538.0 dB/m, 66739.7 dB/m, 59401.6 dB/m, 38275.0 dB/m, and 38275.0 dB/m at the resonance wavelength of 1.281 μm, 1.296 μm, 1.310 μm, 1.329 μm, 1.348 μm, 1.374 μm, and 1.420 μm, respectively, which shows a gradually decreasing trend. The resonance wavelength versus the analyte refractive index is defined as $y = 4295 + 3978x$, and the high linearity R_2 is 0.98. The average sensitivity of the 3rd peak can reach to 3978 nm/RIU. The sensitivity of the 3rd peak of type-1 is higher than that of the 3rd peak of type-2 as the analyte refractive index increases from 1.400 to 1.430. Limited loss spectra of type 2 exhibit higher sensitivity than that of type 1. This is because the energy on the metal surface of the outermost atmospheric hole plays an enhanced role. This stronger surface plasmon resonance is obtained, which meaningfully affects the significant movement of the loss optical fibers. In order to display the resonance wavelength of different analytes more clearly, clear data are shown in Table 2.

The sensitivity is given by

$$S(\lambda) = \frac{\partial \lambda_{\text{peak}}}{\partial n_{\text{a}}} \text{ [nm/RIU]}, \tag{4}$$

where $\partial\lambda_{\text{peak}}$ is the difference between the resonance wavelengths of the two loss spectra for two consecutive analyte refractive indexes and ∂n_{a} is the deference between two analyte refractive indexes. In summary, we analyze the sensitivity of the resonance wavelength to the refractive index by dividing the refractive index from 1.33 to 1.39 and from 1.400 to 1.430. The sensitivity of the 3rd peaks of type-1 and 2 is highly linear. In our article, the sensing characteristics of the PCF are analyzed in detail. When the thickness of the gold nanofilm changes from 40 nm to 80 nm for type-2, the loss of the fundamental mode versus the operation wavelength is shown in Fig. 7. We can find the 1st, 2nd, and 3rd peaks in Fig. 7 when the resonance coupling between the 7th, 6th, 5th SPP modes and the fundamental mode can be obtained. It is firstly demonstrated that the stronger resonance is produced between the high-order SPP mode and the fundamental mode. As shown in Fig. 7, the loss curve is gradually decreasing as the thickness of the gold nanofilm increases from $t_1 = 40$ nm to $t_5 = 80$ nm. The resonance intensities of the 2nd peak are 72633.5 dB/m, 65202.3 dB/m, 55108.5 dB/m, 55020.3 dB/m, and 48173.4 dB/m, respectively. However, the 2nd loss peak shows a weak right movement, and the losses are 85793.9 dB/m, 70014.5 dB/m, 46267.0 dB/m, 48539.9 dB/m, and 44281.6 dB/m, respectively. While the 3rd loss peak exhibits a significant blue shift as the thickness of the gold nanofilm increases from 40 nm to 80 nm, and their values are 74998.2 dB/m, 54971.2 dB/m, 36057.9 dB/m, 19597.5 dB/m, and 13780.4 dB/m, respectively. The resonance intensity is the strongest when the thickness of the gold nanofilm is 40 nm compared to that of other thickness of the gold nano-film. This metal thickness is the most suitable thickness for the preparation of SPR-PCF refractive index sensor. The thinner the metal film, the more free electrons on the surface, and the larger the surface of the metal film. This resonance will be significantly weakened as the thickness of the metal film increases. The correct selection of a suitable film is the basis for better application.

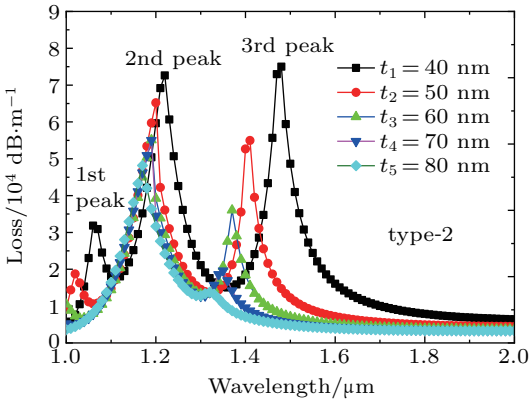

Fig. 7. The loss of fundamental mode in designed PCF for type-2 dependance on the operation wavelength when the thickness of the gold nano-film is 40 nm, 50 nm, 60 nm, 70 nm, and 80 nm.

3. Conclusion

In this paper, we design two SPR-PCF refractive index sensors with wide-range and high-sensitivity based on covering a gold nanofilm around the first cladding air holes. The optical fiber properties of sensing refractive index are studied by increasing the refractive index of the liquid analyte gradually. The sensing properties of the two optical fibers are studied by infiltrating liquid analytes into the outermost air holes. This wide-range analyte liquid is selected to be filled into the two designed PCFs, and the advantages and disadvantages of the two optical fibers sensing characteristics are compared and analyzed. In the simulation process, the FEM is used to analyze and solve the two kinds of optical fiber structures. A large metal film is covered around the first cladding of the optical fiber, which is a novel coating design technology. When the phase matching between the 5th SPP modes and the fundamental mode is met, the resonance coupling can be obtained between the 5th order SPP modes and the fundamental modes. This coating technique leads to the appearance of higher order surface plasmon modes and strong resonance characteristics. As the core mode energy is transferred to the surface of the large gold nanofilm, the 3rd peaks appear at different wavelengths in our simulation. It is observed that the 3rd peaks exhibit a wide-range sensitivity to the analyte refractive index. They are highly consistent with a polynomial fitting law when the refractive index ranges from 1.33 to 1.43. In our simulation, we separately discuss and study the sensitivity of the two

types of PCF with the refractive indexes from 1.33 to 1.39 and from 1.40 to 1.43, and the highest average sensitivity of the 3rd peak is 3978 nm/RIU when the refractive index is from 1.40 to 1.43. The linearity is as high as 0.98.

References

[1] Liu Q, Yan B and Liu J 2019 *Appl. Phys. Express* **12** 052014
[2] Rifat A A, Haider F, Ahmed R, Mahdiraji G A, Mahamd Adikan F R and Miroshnichenko A E 2018 *Opt. lett.* **43** 891
[3] Liu C, Su W, Liu Q, Lu X, Wang F, Sun T and Chu P K 2018 *Opt. Express* **26** 9039
[4] Liu M, Yang X, Shum P and Yuan H 2018 *Appl. Opt.* **57** 1883
[5] Liu C, Yang L, Liu Q, Wang F, Sun Z, Sun T, Mu H and Chu Paul K 2018 *Plasmonics* **13** 779
[6] Yan X, Li B, Cheng T and Li S 2018 *Sensors* **18** 2922
[7] Giorgini A, Avino S, Malara P, Zullo R, De Natale P, Mrkvová K, Homola J and Gagliardi G 2018 *Sens. Actuators B-Chem.* **273** 336
[8] Dash J N and Jha R 2014 *IEEE Photon. Technol. Lett.* **26** 1092
[9] Zhao Y, Deng Z and Wang Q 2014 *Sens. Actuators B-Chem.* **192** 229
[10] Momota M R and Hasan M R 2018 *Opt. Mater.* **76** 287
[11] Chen X, Xia L and Li C 2018 *IEEE Photon. J.* **10** 1
[12] Lu J, Li Y, Han Y, *et al.* 2018 *Appl. Opt.* **57** 5268
[13] Yang Z, Xia L, Li C, Chen X and Liu D 2019 *Opt. Commun.* **430** 195
[14] Liu C, Su W, Wang F, Li X, Liu Q, Mu H, Sun T, Chu Paul K and Liu B 2018 *IEEE Photon. Technol. Lett.* **30** 1471
[15] Luan N, Zhao L, Lian Y and Lou S 2018 *IEEE Photon. J.* **10** 1
[16] Chu S, Nakkeeran K, Abobaker A M, Aphale S S, Babu P R and Senthilnathan K 2018 *IEEE J. Sel. Top. Quant.* **25** 1
[17] Xia Y, Zhang Y, Pan S, Shum P, Yan M, Leviatan Y and Li C 2010 *J. Opt.* **12** 015005
[18] Qian Y, Zhao Y, Wu Q and Yang Y 2018 *Sens. Actuators B-Chem.* **260** 86
[19] Shuai B, Xia L and Liu D 2012 *Opt. Express* **20** 25858
[20] Cao S, Shao Y, Wang Y, Wu T, Zhang L, Huang Y, Zhang F, Liao C, He J and Wang Y 2018 *Opt. Express* **26** 3988
[21] Rifat A A, Mahdiraji G A, Sua Y M, Ahmed R, Shee Y G and Mahamd A F R 2015 *Opt. Express* **24** 2485
[22] Yang Q, Qin L, Cao G, Zhang C and Li X 2018 *Opt. Lett.* **43** 639